DNA Strand Breaks and Denaturation as Probes of Chemical Reactivity versus Thermal Effects of Atmospheric Pressure Plasma Jets

Amal Sebastian, Daniel Lipa, and Sylwia Ptasinska*

ACCESS | Metrics & More | Article Recommendations | Supporting Information

ABSTRACT: An atmospheric pressure plasma jet (APPJ) is being advanced as an alternative radiation type that offers excellent efficacy in an array of medical applications against specific biological targets such as DNA. This work explores the possibility of implementing DNA and its damage as a probe for specific plasma diagnostics such as reactive plasma species formation and transient local heating. We analyzed both APPJ characteristics based on the detection of plasma-induced strand breaks and DNA denaturation. Further, we implemented a machine learning model based on artificial neural networks to predict the type and extent of DNA damage for a given combination of APPJ parameter values. This methodology is an important step toward deciphering and explaining the potential adverse effects of APPJ on biological samples of any prospective interest in medicine.
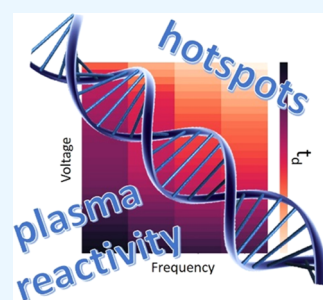
INTRODUCTION

Plasma that forms based on dielectric barrier discharge ignited at atmospheric pressure is a source of many reactive species and other plasma components that can interact chemically and physically with any potential target at close to room temperature. The presence of enormous numbers of reactive, but nonthermal species and the ability to deliver them to any target have made atmospheric pressure plasma jets (APPJs) attractive radiation sources for versatile applications ranging from medicine to material processing. Specifically, in medical treatment, it may be beneficial in bacterial and viral inactivation,[1−3] and has already proven its effectiveness in cancer therapy,[4−6] wound healing and disinfection,[5,7−10] and other related applications.

The rapid growth of clinical trials of APPJ in recent years has accompanied the remarkable progress in understanding plasma's biological effects on living cells and their components at the molecular level. Moreover, plasma radiation's efficacy can be tuned and optimized for a specific biological outcome by varying values of the plasma source parameters.[11] These numerous parameters may include the type of discharge, voltage applied to the electrode, plasma power, frequency, feed gas flow rate, plasma−target distance, irradiation time, and target properties.[12−17] Thus, the thorough assessment of the correlation between plasma parameters and biological effects has always been a critical factor in determining APPJs for any medical application.

Our previous research focused extensively on plasma-induced strand breaks in an aqueous DNA molecule induced by various plasma components,[12,13] particularly reactive oxygen and nitrogen species in APPJ because of their significant biological activities.[6,14] Our results indicated that
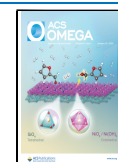
the extent of strand break formation, which results from bond breakage in one (single-strand break, SSB) or two (double-strand break, DSB) backbones of the DNA helix, can be varied promptly by tuning plasma parameter values because of DNA's susceptibility to all plasma components.[16] In this work, we report experimental results on DNA damage when exposed to APPJ generated at a much more extensive range of plasma parameter values. This improved technical capability allowed us to observe previously undetected DNA denaturation, in which the DNA helix unfolds and splits into two single strands, in addition to the DNA strand breaks upon plasma irradiation. Thus, our primary focus has been to determine whether DNA denaturation, known to occur during heating,[18,19] may be a reliable indicator of the plasma's elevated gas temperature when thermal effects in biological targets suppress the plasma reactivity. Nonthermal effects, such as a pH-mediated process, can also cause denaturation in the alkaline environment[20,21] but it can be ruled out as plasma-treated liquids have an acidic pH.[22−24]

To support our experimental findings, we used a predictive model using specific machine learning (ML) algorithms that we applied to predict plasma-induced changes in DNA accurately for a given combination of APPJ parameter values. We designed and implemented the predictive models based on ML algorithms and artificial neural networks (ANNs)
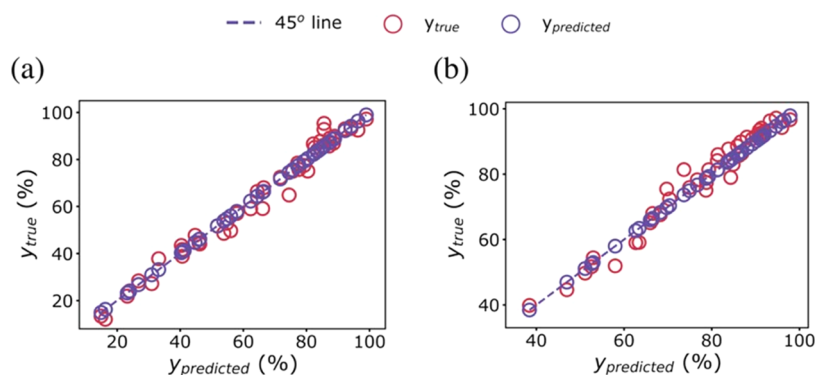
Figure 1. Predictive modeling of plasma-induced DNA damage. (a) Plot of predicted versus true values for the extent of strand break formation as modeled with the ANN. Evaluation metrics: mean absolute error (MAE) = 2.52, root-mean-square error (RMSE) = 3.52, and coefficient of statistic determination, R^2 = 0.98. (b) Plot of predicted versus true values for the extent of total DNA damage as modeled with the PGNN. Evaluation metrics: MAE = 1.89, RMSE = 2.54, and R^2 = 0.98.

previously to model the type and extent of DNA damage.[25] However, our previous work emphasized primarily the evaluation of the plasma dose rate and its changes depending on plasma parameters. What remains unexplored is the possibility of performing plasma jet diagnostics based on the changes induced in the target. To accomplish this, we broaden the exciting possibility of ML-based models to predict DNA denaturation, thus to determine APPJ parameters at which the transition between plasma reactivity and thermal effects can occur. Therefore, in contrast to the previous work,[25] we here investigated the prospect of revealing the correlation between DNA damage and plasma properties that can serve as plasma diagnostics, i.e., plasma gas temperature and reactive species formation, that was also supported by predictive modeling of DNA denaturation.

■ RESULTS AND DISCUSSION

In our experimental study, we used plasmid DNA (Note S1), as a molecular probe, that was irradiated by helium-fed APPJ produced by a custom-made plasma source (Figure S1). We followed a statistical experimental design, also known as the design of experiments (DoE), to acquire the data necessary to generate predictive models. The DoE matrix based on the experiments performed was generated from the combinations of four crucial APPJ parameters that influence plasma-induced changes in DNA significantly, i.e., voltage applied, frequency, irradiation time, and feed gas flow rate. For each combination of plasma parameters in the DoE matrix (Table S1), the extent of plasma-induced strand breaks, i.e., SSBs and DSBs, and total DNA damage, which includes the occurrence of both types of strand breaks and denaturation, was quantified using a gel electrophoresis technique[12,13] (Notes S3 and S4).

After a large number of experimental data acquired via the DoE were collected, we split the data into training and testing data and implemented training data in the standard supervised ML workflow.

Similarly to our previous work,[25] we designed several predictive models (Note S5) to determine the extent of possible types of DNA damage for a given combination of APPJ parameter values. As we discussed later, different types of DNA damage showed different trends in their extent as a function of irradiation time. While, the total plasma-induced DNA damage increased with the increase in irradiation time, as shown in Figure S2. Therefore, we created a pure ANN architecture for the predictive modeling of the strand break

formation, while in the case of the total plasma-induced DNA damage, we used a physics-guided neural network (PGNN)[26] (Note S6). Using PGNN, which includes a physical loss function (PHYLOSS) allowed us to capture any violation of physics laws obtained in our modeling. Thus, the model predictions for data points that indicated a more significant extent of DNA damage for a shorter time than the one for a longer irradiation time was penalized by employing the PHYLOSS (see Note S6). The inclusion of PHYLOSS function yielded the PGNN model, which showed physically consistent predictions for the extent of DNA damage that increased with prolonged irradiation times.

Further, the data distribution of the extent of DNA damage created from the DoE matrix revealed rare values of either DNA strand break formation or total DNA damage in the data within a short irradiation time (Figures S3 and S4). Rare values that correspond to the minority data were oversampled during the refinement stage of the ML workflow using the synthetic minority oversampling method (SMOTE).[27] Next, we performed hyperparameter optimization of both the ANN and PGNN models using the grid-search cross-validation method for strand break formation and total DNA damage (Tables S2 and S3). Then, we evaluated the optimized ANN and PGNN models of the test data, as shown in Figure 1a,b. The predictive models performed well on the test data with root-mean-square error (RMSE) and R^2 scores of 3.52 and 0.98 for the extent of strand break formation (Figure 1a) and scores of 2.54 and 0.98, respectively, for the extent of total DNA damage (Figure 1b) as computed using the ANN and PGNN models, respectively. Further, the PHYLOSS for PGNN was zero after the model was refined, proving that modeling the extent of total DNA damage with PGNN was physically consistent, as detailed in Note S6.

Because the nonaugmented test dataset was relatively small, we also attempted to assess the model's performance with a large augmented test dataset. Although evaluations with oversampled test datasets are not implemented typically, we assessed whether the model performed well for an extensive test dataset. The model evaluations with the larger dataset showed excellent outcomes, the results of which are presented in Figure S5.

After we generated the ANN and PGNN models, we assessed the influence of several APPJ parameters, such as the voltage applied, plasma frequency, and power, on the extent of plasma-induced DNA damage based on our ML-based
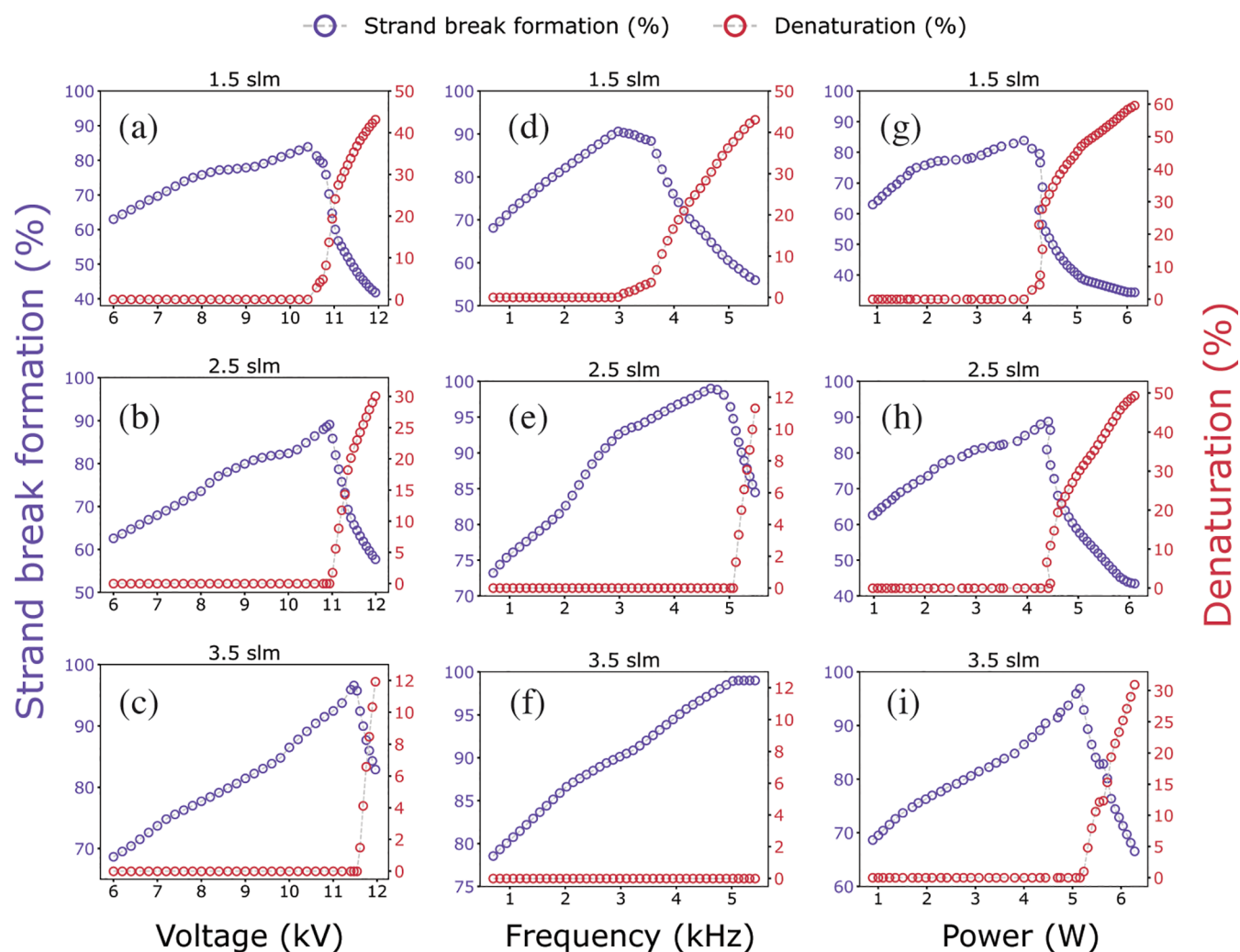
Figure 2. Predictive modeling of DNA damage versus plasma parameters. (a−c) Plots of predicted strand break formation and denaturation as a function of voltage modeled with the ANN and PGNN at three different flow rates, 1.5, 2.5, and 3.5 slm, respectively, and at the frequency of 2 kHz. (d−f) Plots as above but as a function of frequency at the voltage of 10 kV. (g−i) Plots as above but as a function of power at the frequency of 2 kHz. The irradiation time was 25 s for all plots.

predictive models. As discussed later, having the dependencies for strand break formation and denaturation as a function of these parameters allowed us to gain qualitative insights into the transition point at which effects attributable to the thermal effects begin to be detectable in addition to the effects due to plasma's reactivity. Here, the dependencies for DNA denaturation were acquired by subtracting the extent of strand breaks modeled using the ANN from the extent of total DNA damage modeled using the PGNN. The results of the predictive modeling of DNA damage, i.e., strand break formation and denaturation, are presented in Figure 2 and show their dependence on voltage, frequency, and power for selected combinations of plasma parameters.

Figure 2a−c displays the results for strand break formation and denaturation as a function of plasma voltage that ranged from 6 to 12 kV at three flow rates. In the case of plasma-induced strand breaks that occurred below 10 kV, the modeled results showed the gradual increase in this type of damage with increased voltage. This increase in the extent of DNA strand breaks derives from the interaction of plasma reactive species, which was reported in our previous study.[28] In our previous study, in which DNA and a chemical dosimeter, i.e., Fricke

solution, were irradiated by APPJ using the same plasma source as in this study, we observed similar increasing trends with an increase in voltage both for strand break formation detected in DNA and for the total yields of reactive species detected in the chemical dosimeter.[28] Therefore, the formation of strand breaks in DNA was attributed to the presence of reactive species injected into the target and formed in the liquid during plasma irradiation.

Above 10 kV, the modeled results showed that the strand break formation is quenched abruptly with the simultaneous appearance of DNA denaturation. The combination of plasma parameters at which the decrease in strand break formation and the increase in denaturation are observed, we indicate as a transition point. Because the primary reason for the formation of denatured DNA is heating,[18,19] the appearance of the transition point implies that plasma gas temperature increases as the voltage applied increases. To verify the changes in plasma temperatures with the voltage, we performed measurements of APPJ gas temperature using a temperature sensor (Note S7). As presented later, an increase in voltage caused the plasma gas temperature to increase.
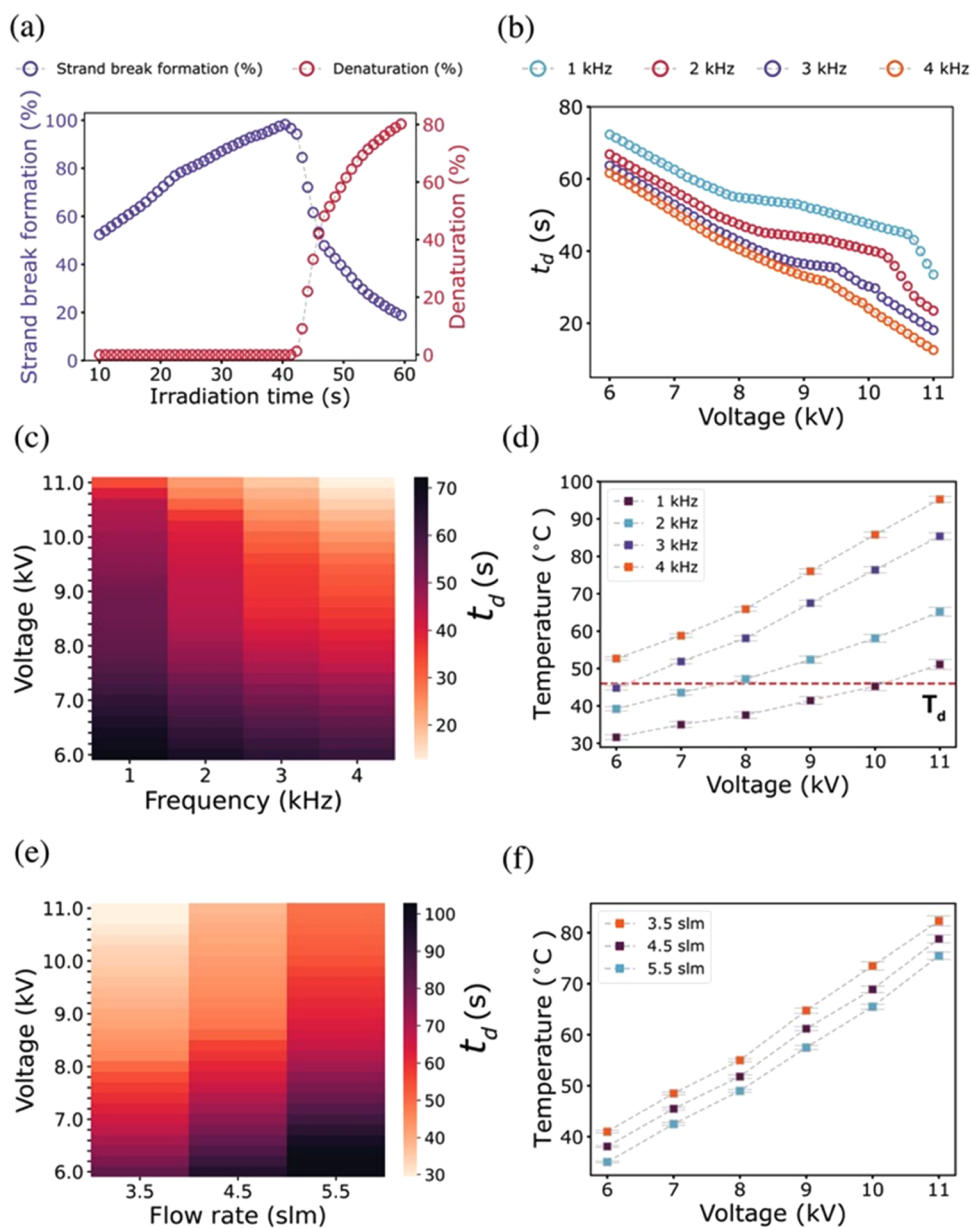
Figure 3. Transition point and its evolution with voltage, frequency, and flow rate. (a) Example of predicted strand break formation and denaturation as a function of irradiation time with APPJ parameters of 9.5 kV, 2 kHz, and 2 slm. (b) Plot of the irradiation time required for DNA to denature (t_d) as a function of voltage for four different frequencies, 1, 2, 3, and 4 kHz, at the flow rate of 2 slm. (c) Heatmap of t_d as a function of voltage and frequency at the flow rate of 2 slm. (d) APPJ temperature measurements performed for voltages from 6 to 11 kV and frequencies from 1 to 4 kHz at the flow rate of 2 slm. (e) Heatmap of t_d as a function of voltage and flow rates at the frequency of 3 kHz. (f) APPJ temperature measurements performed for voltages from 6 to 11 kV and flow rates from 3.5 to 5.5 slm at the frequency of 3 kHz.

Further, our predictive model revealed that the transition point shifts toward higher voltages with an increased flow rate. For a low flow rate, i.e., 1.5 standard liters per minute (slm), the denaturation is predicted to occur at ~10.5 kV, and for 3.5 slm, it occurred at 11.5 kV when the frequency was maintained at 2 kHz in both cases, implying a cooling effect of plasma gas with higher flow rates.

Figure 2d−f displays the results of the predictive models for strand break formation and denaturation as a function of plasma frequency in the range of 1−5.5 kHz at three flow rates. The voltage was held constant at 10 kV for all of these predictions. The results showed that plasma-induced strand breaks were predicted to increase with frequency in lower frequency ranges, while DNA denaturation was expected to

occur at higher frequencies. Moreover, the transition point between the two types of damage shifts toward higher frequencies at higher flow rates. Similar to the effect of the low-voltage applied, denaturation occurred at relatively lower frequency values at lower flow rates, i.e., ~3 kHz at 1.5 slm, 5 kHz at 2.5 slm, and no denaturation occurred within the maximum frequency range (5 kHz) at 3.5 slm.

Further, the average instantaneous plasma power per pulse was estimated from the I−V characteristics (Note S8 and Figure S1) for each combination of APPJ parameter values. The plasma-induced DNA damage for selected APPJ parameter values is plotted as a function of plasma power in Figure 2g−i. Because the plasma frequency was held constant the same for these predictions, the power dependencies

showed relatively similar trends as the voltage dependencies. Thus, the strand break formation occurred in a low plasma power region, i.e., below 4 W, and the higher power that results from higher voltages causes DNA denaturation. The transition point occurred at relatively lower power values with lower flow rates, i.e., ~4 W at 1.5 slm, 4.5 W at 2.5 slm, and 5.25 W at 3.5 slm.

All three dependencies modeled and presented in Figure 2 were performed at a specific irradiation time, i.e., 25 s, and showed that the transition point between the two types of DNA damage can vary depending on voltage, frequency, power, and flow rate. To assess the irradiation time's effect on DNA damage and provide a time at which the transition point occurs, we modeled the extents of plasma-induced strand break formation and denaturation for several combinations of APPJ parameter values as a function of time (Figure 3).

For example, Figure 3a shows the formation of strand breaks and denatured DNA predicted as a function of irradiation time at 9.5 kV, 2 kHz, and 2 slm with a transition point at ~40 s. As our modeling showed, the irradiation time required for denaturation to occur (t_d) varied for different APPJ parameter value combinations. The evolution of this transition time as a function of voltage for several frequency values was computed from the predictive model. Figure 3b,c represents the plot and heatmap, respectively, for changes in the transition time computed for voltages from 6 to 11 kV and frequencies from 1 to 4 kHz at the flow rate of 2 slm. As the figure shows, t_d decreased with an increase in the voltage applied and frequency. The longest t_d was ~75 s at a voltage of 6 kV and frequency of 1 kHz, and the shortest one was 10 s at 11 kV and 4 kHz. Because denaturation results from thermal effects, the increase in the voltage applied and frequency implies the APPJ temperature elevation, and thus the increase in the heat transfer rate at higher voltages and frequencies, which consequently leads to lower t_d values. To confirm the correlation between the transition time and its shifts with plasma parameters with potential changes in APPJ temperature, we performed direct measurements of the plasma gas temperature at different voltages and frequencies. Figure 3d shows the temperatures measured as a function of voltage in the range from 6 to 11 kV for four frequency values. As seen in the figure, at the lowest voltage and frequency measured, i.e., 6 kV and 1 kHz, the plasma temperature reaches only 30 °C. The increase in both parameters elevates the APPJ temperature up to even 100 °C at 11 kV and 4 kHz. It is important to notice, that we investigated the formation of denatured DNA experimentally when the plasmid DNA used in our experiments was heated over a range of temperatures (37−65 °C) (Note S1). We observed no DNA denaturation at 37 °C, while some extent of denatured DNA was present at 45 °C. Therefore, in Figure 3d, we also show the temperature of DNA at which we began to observe denaturation experimentally, T_d. Other studies have also reported thermal denaturation of plasmid DNA at similar temperatures;[18,19] however, this temperature can shift according to the type of plasmid DNA, its structure and sequence, buffer used, etc.[29]

We also assessed the flow rate's effect on the shifts in transition points and plasma gas temperature. The heatmap in Figure 3e represents changes in the transition points, which we computed using the predictive model for three different flow rates, 3.5, 4.5, and 5.5 slm, and voltages from 6 to 11 kV, while the frequency was held constant at 3 kHz. The results indicated that the transition point occurs after a longer

irradiation time at higher flow rates. This is attributable to the decrease in APPJ's temperature with an increase in the flow rate, as was measured and is presented in Figure 3f. We observed a decline of ~4 °C for each 1 slm increase in the flow rate, indicating a cooling effect in the case of higher flow rates.

Our results described above demonstrated the possibility of identifying APPJ's chemical reactivity versus its thermal effects by assessing DNA damage and combining these experimental evidence with the predictive model for a wide range of plasma parameter values. To obtain information about both properties, we identified the formation of strand breaks caused by plasma reactive species interaction and denatured DNA caused by thermal effects in the sample irradiated with different combinations of plasma parameter values. Further, using predictive modeling, we obtained the evolution of these two types of DNA damage as a function of voltage (and power), frequency, flow rate, and irradiation time (Figures 2 and 3). Here, we will provide the physicochemical interpretation of the obtained results to emphasize the significance of our methodology as a diagnostic of plasma chemical reactivity versus its thermal effect, particularly the transition point at which temperature-caused denaturation is detectable.

In the case of voltage dependence, the strand break formation was predicted to occur at relatively low voltages and increased gradually with higher voltages until the transition point above which denaturation was a more dominant process (Figure 2a−c). The increase in the extent of strand breaks in DNA was correlated with an increase in reactive species delivered from APPJ and formed in the sample. However, above the transition point, the increase in denatured DNA formation indicated elevated plasma gas temperatures at higher voltages, which was confirmed by the APPJ temperature measurements (Figure 3d). Achieving higher temperatures can be explained by an enhancement of electron impact processes as the power increased[30] caused by the increase in the amplitude of the voltage. Thus, more energy is dissipated by the plasma, promoting the energy transferred to gas molecules through collisions with charged species. Importantly, the changes in the voltage affect the electric field, which is associated with ionization front propagation[31,32] and which can have significant implications in biological systems.[33]

Similar trends in DNA damage were predicted in the case of frequency dependence, in which an increased frequency induced more strand breaks in DNA until the transition point at which the denaturation process became the predominant type of damage. The increase in DNA damage overall can be attributed again to the increase in reactive species until the temperature is sufficient to induce denaturation. Indeed, as we measured, the APPJ's temperature increased as the frequency increased (Figure 3d). The frequency's effect on gas temperature, which was established previously,[34,35] originates from the fact that higher frequencies give rise to larger numbers of plasma pulses during irradiation. Given that electrons and, consequently, gas molecules, gain energy from collisions during each plasma pulse, plasma gas temperatures arise at higher frequencies.

Further, for both voltage and frequency dependencies, we investigated the effect of the flow rate on the extent of DNA damage. On the one hand, we found that an increase in the flow rate caused more strand breaks, which can be attributed to a larger number of reactive species delivered to the irradiated sample. The effect of flow rate on the formation of plasma reactive species was investigated by several groups and

confirmed the increase of certain species in a specific range of flow rates.[36,37] However, on the other hand, in the case of denaturation, the transition point shifted toward a higher voltage or frequency, implying that the higher flows cause the gas cooling. We confirmed this by the measurement of APPJ temperature as well (Figure 3f). A decrease in plasma temperature with increased flow rates was reported in previous studies and was attributed to a convective cooling effect with gas flow, in which energy is lost by colliding gas molecules having their energy gained earlier from collisions with charged species, thus decreasing the gas temperature.[34,35]

In addition to plasma parameter dependencies on DNA damage, we were able to predict the transition point, and therefore, identify the combination of APPJ parameter values at which plasma's thermal effects begin to be considerable in addition to its reactivity. As was introduced above, the transition point corresponds to the irradiation time necessary for denaturation to occur for a given combination of APPJ parameter values. Figure 3c,e presents heatmaps of the transition point evolution computed as a function of two parameters, i.e., voltage and either frequency or flow rate, respectively. These heatmaps allowed us to determine the APPJ conditions for DNA irradiation at which there are minimal temperature-induced effects. Thus, we were able to identify the conditions under which any rapid and local increase in the temperature that could potentially denature DNA can be avoided. For example, the APPJ temperature measured at a voltage of 8 kV, frequency of 1 kHz, and flow rate of 2 slm was 35 °C, which would indicate that these conditions are safe for irradiation and no thermal effects could be induced because this temperature is far below the T_d for DNA (Figure 3d). However, based on the heatmap computed in Figure 3c, the transition point corresponds to 50 s for 8 kV, 1 kHz, and 2 slm, and thus, plasma irradiation longer than t_d will induce thermal effects even if the APPJ gas temperature overall is lower than that for DNA denaturation to occur. A similar effect, DNA denaturation at low (room) temperatures, was observed recently when DNA was irradiated with nonionizing microwave and terahertz radiation.[38] Both types of radiation can excite and induce oscillation in DNA, and rupture hydrogen bonds between the base pair of double-stranded DNA that results in denaturation. Therefore, these structural changes in DNA were attributed to transient local heating of the aqueous DNA, referred to as "hotspots", while bulk heating was not observed. Such bulk heating was prevented by efficient cooling with the liquid heat sink in the case of microwaves and in the case of terahertz, pulses of a short duration.[38] In our previous study, we reported that during plasma discharge of a short duration that occurs only at the rising and falling voltage edges (Figure S1b), the energy is within the range of a few millijoules per pulse.[35] Indeed, similar to microwave and terahertz energy, this energy can be pumped quickly into the sample as heat before reaching equilibrium. Therefore, our temperature measurements by conventional thermal probes were not sufficiently rapid to record such a transient increase in temperature.

Further, our methodology allowed us to propose potential parameter values that may be ideal for applications in which plasma temperature-induced effects must be avoided. For example, because plasma-induced DNA damage serves as the basis for several plasma medical applications, such as cancer therapy, our modeling can inform the identification of optimal APPJ parameters of potential interest to medicine. Based on

our predictive modeling, we were able to provide a specific combination of plasma parameter values that could damage DNA significantly and produce different types of damage, such as SSB, DSB, and denaturation. Among those, DSBs play a particularly pivotal role in inducing apoptosis in cancer cells,[39−41] which can be induced by reactive species introduced during plasma irradiation while preventing any thermal effects simultaneously.

One of the potential combinations of APPJ parameter values that lead to the greatest extent of DSB formation is presented in Figure 4. These DSB results were obtained using predictive
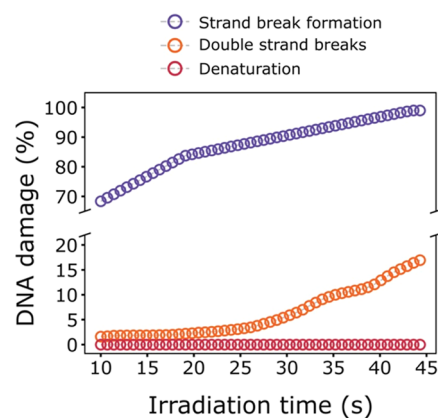

Figure 4. Proposed optimal combination of APPJ parameter values for potential medical applications. The plot of predicted plasma-induced DNA damage with a particular focus on DSB formation as a function of irradiation time for the following APPJ parameter values, 4.5 slm, 9 kV, and 3.5 kHz. Our modeling shows no occurrence of denaturation over the treatment time window used in our experiments for this parameter choice.

modeling, which was evaluated as shown in Figure S6, while the extents of strand break formation and denaturation were modeled as described above. As was mentioned above already, for plasma medical applications, it is also undesirable to use APPJ parameter value combinations that lead to higher plasma temperatures. Therefore, a high flow rate regime was considered an optimal choice, as it provides a relatively low gas temperature (see Figure 3f). As shown in Figure 4, ∼98% of DNA damage, including 15%, which was attributed to the DSB formation, is predicted to occur at an irradiation time of 45 s for a relatively high voltage and frequency combination, i.e., 9 kV and 3.5 kHz. Such an extent of DSB formation is considered to be substantial, given that no denaturation is occurring in the target simultaneously during plasma irradiation.

■ CONCLUSIONS

In summary, we proposed employing DNA that acts as a unique molecular probe for unprecedented plasma diagnostic purposes and combining our experimental findings with ML modeling of the extent of DNA denaturation. Using this methodology, we were able to model and predict APPJ parameters at which the formation of different types of damage occurred during plasma irradiation, thus indicating the damage induced due to thermal and/or chemical properties. This methodology is superior to traditional techniques for temperature measurements using any sensor, such as thermometers, thermocouples, and any digital thermal probes because it reveals the occurrence of transient local heating in the sample.

Moreover, our modeling revealed combinations of plasma parameters that correspond to temperatures that are below thermal denaturation, yet at which denatured DNA can still occur. This is a critical aspect to take into consideration for plasma applications that involve temperature-sensitive targets.

ASSOCIATED CONTENT

Supporting Information

The Supporting Information is available free of charge at https://pubs.acs.org/doi/10.1021/acsomega.2c07262.

> Additional experimental details, including experimental setup and its characterization, sample preparation and analysis, and computational details, including model descriptions, with associated figures and tables (PDF)

AUTHOR INFORMATION

Corresponding Author

Sylwia Ptasinska − *Radiation Laboratory, University of Notre Dame, Notre Dame, Indiana 46556, United States; Department of Physics and Astronomy, University of Notre Dame, Notre Dame, Indiana 46556, United States;* orcid.org/0000-0002-7550-8189; Email: sptasins@nd.edu

Authors

Amal Sebastian − *Radiation Laboratory, University of Notre Dame, Notre Dame, Indiana 46556, United States; Department of Physics and Astronomy, University of Notre Dame, Notre Dame, Indiana 46556, United States*

Daniel Lipa − *Radiation Laboratory, University of Notre Dame, Notre Dame, Indiana 46556, United States; Department of Applied and Computational Mathematics and Statistics, University of Notre Dame, Notre Dame, Indiana 46556, United States*

Complete contact information is available at:
https://pubs.acs.org/10.1021/acsomega.2c07262

Notes

The authors declare no competing financial interest.

ACKNOWLEDGMENTS

REFERENCES

(1) Bisag, A.; Isabelli, P.; Laurita, R.; Bucci, C.; Capelli, F.; Dirani, G.; Gherardi, M.; Laghi, G.; Paglianyi, A.; Sambri, V.; Colombo, V. Cold atmospheric plasma inactivation of aerosolized microdroplets containing bacteria and purified SARS-CoV-2 RNA to contrast airborne indoor transmission. *Plasma Processes Polym.* **2020**, *17*, 2000154.

(2) Guo, L.; Yao, Z.; Yang, L.; Zhang, H.; Qi, Y.; Gou, L.; Xi, W.; Liu, D.; Zhang, L.; Cheng, Y.; Wang, X.; Rong, M.; Chen, H.; Kong, M. G. Plasma-activated water: An alternative disinfectant for S protein inactivation to prevent SARS-CoV-2 infection. *Chem. Eng. J.* **2021**, *421*, 127742.

(3) Mohamed, H.; Nayak, G.; Rendine, N.; Wigdahl, B.; Krebs, F. C.; Bruggeman, P. J.; Miller, V. Non-Thermal Plasma as a Novel Strategy for Treating or Preventing Viral Infection and Associated Disease. *Front. Phys.* **2021**, *9*, 683118.

(4) von Woedtke, T.; Laroussi, M.; Gherardi, M. Foundations of plasmas for medical applications. *Plasma Sources Sci. Technol.* **2022**, *31*, No. 054002.

(5) Boeckmann, L.; Schäfer, M.; Bernhardt, T.; L Semmler, M. L.; Jung, O.; Ojak, G.; Fischer, T.; Peters, K.; Nebe, B.; Müller-Hilke, B.; Seebauer, C.; Bekeschus, S.; Emmert, S. Cold Atmospheric Pressure Plasma in Wound Healing and Cancer Treatment. *Appl. Sci.* **2020**, *10*, 6898.

(6) Alizadeh, E.; Ptasińska, S. Recent Advances in Plasma-Based Cancer Treatments: Approaching Clinical Translation through an Intracellular View. *Biophysica* **2021**, *1*, 48−72.

(7) Bekeschus, S.; Schmidt, A.; Weltmann, K. D.; von Woedtke, T. The plasma jet kINPen − A powerful tool for wound healing. *Clin. Plasma Med.* **2016**, *4*, 19−28.

(8) Bernhardt, T.; Semmler, M. L.; Schäfer, M.; Bekeschus, S.; Emmert, S.; Boeckmann, L. Plasma Medicine: Applications of Cold Atmospheric Pressure Plasma in Dermatology. *Oxid. Med. Cell. Longevity* **2019**, *2019*, 3873928.

(9) Maho, T.; Binois, R.; Morabito, F. B.; Demasure, M.; Douat, C.; Dozias, S.; Bocanegra, P. E.; Goard, I.; Hocqueloux, H.; Helloco, C. L.; Orel, I.; Pouvesle, J. M.; Prazuck, T.; Stancampiano, A.; Tocaben, C.; Robert, E. Anti-Bacterial Action of Plasma Multi-Jets in the Context of Chronic Wound Healing. *Appl. Sci.* **2021**, *11*, 9598.

(10) Daeschlein, G.; Napp, M.; Lutze, S.; Arnold, A.; von Podewils, S.; Guembel, D.; Junger, M. Skin and wound decontamination of multidrug-resistant bacteria by cold atmospheric plasma coagulation. *J. Deutsch. Dermatol. Ges.* **2015**, *13*, 143−150.

(11) Morabit, Y.; Hasan, M. I.; Whalley, R. D.; et al. A review of the gas and liquid phase interactions in low-temperature plasma jets used for biomedical applications. *Eur. Phys. J. D* **2021**, *75*, 32.

(12) Han, X.; Cantrell, W. A.; Escobar, E. E.; Ptasinska, S. Plasmid DNA damage induced by helium atmospheric pressure plasma jet. *Eur. Phys. J. D* **2014**, *68*, 46.

(13) Adhikari, E. R.; Ptasinska, S. Correlation between helium atmospheric pressure plasma jet (APPJ) variables and plasma induced DNA damage. *Eur. Phys. J. D* **2016**, *70*, 180.

(14) Khlyustova, A.; Labay, C.; Machala, Z.; Ginebra, M. P.; Canal, C. Important parameters in plasma jets for the production of RONS in liquids for plasma medicine: A brief review. *Front. Chem. Sci. Eng.* **2019**, *13*, 238−252.

(15) Li, G.; Li, H. P.; Wang, L. Y.; Wang, S.; Zhao, H. X.; Sun, W. T.; Xing, X. H.; Bao, C. Y. Genetic effects of radio-frequency, atmospheric-pressure glow discharges with helium. *Appl. Phys. Lett.* **2008**, *92*, No. 221504.

(16) Arjunan, K. P.; Sharma, V. K.; Ptasinska, S. Effects of Atmospheric Pressure Plasmas on Isolated and Cellular DNA—A Review. *Int. J. Mol. Sci.* **2015**, *16*, 2971−3016.

(17) Adhikari, E. R.; Samara, V.; Ptasinska, S. Influence of O_2 or H_2O in a plasma jet and its environment on plasma electrical and biochemical performances. *J. Phys. D: Appl. Phys.* **2018**, *51*, No. 185202.

(18) Yan, L.; Iwasaki, H. Thermal Denaturation of Plasmid DNA Observed by Atomic Force Microscopy. *Jpn. J. Appl. Phys.* **2002**, *41*, 7556−7559.

(19) Víglaský, V.; Antalík, M.; Adamčík, J.; Podhradský, D. Early melting of supercoiled DNA topoisomers observed by TGGE. *Nucleic Acids Res.* **2000**, *28*, No. e51.

(20) Ageno, M.; Dore, E.; Frontali, C. The alkaline denaturation of DNA. *Biophys. J.* **1969**, *9*, 1281−1311.

(21) Wang, X.; Lim, H. J.; Son, A. Characterization of denaturation and renaturation of DNA for DNA hybridization. *Envion. Health Toxicol.* **2014**, *29*, No. e2014007.

(22) Helmke, A.; Hoffmeister, D.; Mertens, N.; Emmert, S.; Schuette, J.; Vioel, W. The acidification of lipid film surfaces by non-thermal DBD at atmospheric pressure in air. *New J. Phys.* **2009**, *11*, No. 115025.

(23) Jablonowski, H.; von Woedtke, T. Research on plasma medicine-relevant plasma−liquid interaction: What happened in the past five years? *Clin. Plasma Med.* **2015**, *3*, 42−52.

(24) Rezaei, F.; Vanraes, P.; Nikiforov, A.; Morent, R.; De Geyter, N. Applications of Plasma-Liquid Systems: A Review. *Materials* **2019**, *12*, 2751.

(25) Sebastian, A.; Spulber, D.; Lisouskaya, A.; Ptasinska, S. Revealing low-temperature plasma efficacy through a dose-rate assessment by DNA damage detection combined with machine learning models. *Sci. Rep.* **2022**, *12*, No. 18353.

(26) Daw, A.; Karpatne, A.; Watkins, W.; Read, J.; Kumar, V. Physics-guided Neural Networks (PGNN): An Application in Lake Temperature Modeling, 2017. arXiv:1710.11431. https://arxiv.org/abs/1710.11431.

(27) Torgo, L.; Branco, P.; Ribeiro, R. P.; Pfahringer, B. Resampling strategies for regression. *Expert Syst.* **2015**, *32*, 465−476.

(28) Adhikari, E. R.; Samara, V.; Ptasinska, S. Total yield of reactive species originating from an atmospheric pressure plasma jet in real time. *Biol. Chem.* **2018**, *400*, 93−100.

(29) Bettotti, P.; Visone, V.; Lunelli, L.; Perugino, G.; Ciaramella, M.; Valenti, M. Structure and Properties of DNA Molecules Over The Full Range of Biologically Relevant Supercoiling States. *Sci. Rep.* **2018**, *8*, No. 6163.

(30) Ozkan, A.; Dufour, T.; Silva, T.; Britun, N.; Snyders, R.; Bogaerts, A.; Reniers, F. The influence of power and frequency on the filamentary behavior of a flowing DBD—application to the splitting of CO_2. *Plasma Sources Sci. Technol.* **2016**, *25*, No. 025013.

(31) Robert, E.; Darny, T.; Dozias, S.; Iseni, S.; Pouvesle, J. M. New insights on the propagation of pulsed atmospheric plasma streams: From single jet to multi jet arrays. *Phys. Plasmas* **2015**, *22*, No. 122007.

(32) Bourdon, A.; Darny, T.; Pechereau, F.; Pouvesle, J. M.; Viegas, P.; Iséni, S.; Robert, E. Numerical and experimental study of the dynamics of a μs helium plasma gun discharge with various amounts of N_2 admixture. *Plasma Sources Sci. Technol.* **2016**, *25*, No. 035002.

(33) Vijayarangan, V.; Delalande, A.; Dozias, S.; Pouvesle, J.-M.; Robert, E.; Pichon, C. New insights on molecular internalization and drug delivery following plasma jet exposures. *Int. J. Pharm.* **2020**, *589*, No. 119874.

(34) Svarnas, P.; Papadopoulos, P. K.; Athanasopoulos, D.; Sklias, K.; Gazeli, K.; Vafeas, P. Parametric study of thermal effects in a capillary dielectric-barrier discharge related to plasma jet production: Experiments and numerical modelling. *J. Appl. Phys.* **2018**, *124*, No. 064902.

(35) Samara, V.; Sutton, Y.; Braithwaite, N.; Ptasinska, S. Acoustic characterization of atmospheric-pressure dielectric barrier discharge plasma jets. *Eur. Phys. J. D* **2020**, *74*, 169.

(36) Tang, Q.; Jiang, W.; Cheng, Y.; Lin, S.; Lim, T. M.; Xiong, J. Generation of Reactive Species by Gas-Phase Dielectric Barrier Discharges. *Ind. Eng. Chem. Res.* **2011**, *50*, 9839−9846.

(37) Baek, E. J.; Joh, H. M.; Kim, S. J.; Chung, T. H. Effects of the electrical parameters and gas flow rate on the generation of reactive species in liquids exposed to atmospheric pressure plasma jet. *Phys. Plasmas* **2016**, *23*, No. 073515.

(38) Greschner, A. A.; Ropagnol, X.; Kort, M.; Zuberi, N.; Perreault, J.; Razzari, L.; Ozaki, T.; Gauthier, M. A. Room-Temperature and Selective Triggering of Supramolecular DNA Assembly/Disassembly by Nonionizing Radiation. *J. Am. Chem. Soc.* **2019**, *141*, 3456−3469.

(39) Han, X.; Klas, M.; Liu, Y.; Stack, M. S.; Ptasinska, S. DNA damage in oral cancer cells induced by nitrogen atmospheric pressure plasma jets. *Appl. Phys. Lett.* **2013**, *102*, No. 233703.

(40) Lips, J.; Kaina, B. DNA double-strand breaks trigger apoptosis in p53-deficient fibroblasts. *Carcinogenesis* **2001**, *22*, 579−585.

(41) Roos, W. P.; Kaina, B. DNA damage-induced cell death by apoptosis. *Trends Mol. Med.* **2006**, *12*, 440−450.